RSC Advances

ROYAL SOCIETY OF CHEMISTRY

www.rsc.org/advances

Self-assembling nano mixed-brushes having co-continuous surface morphology by melt growing single crystals and comparison with solution patterned leopard-skin surface morphology

S. Agbolaghi[a,b], M. Alizadeh-Osgouei[a,b], S. Abbaspoor[a,b], F. Abbasi[a,b,*]

[a] Institute of Polymeric Materials, Sahand University of Technology, Tabriz, Iran

[b] Faculty of Polymer Engineering, Sahand University of Technology, Tabriz, Iran

Abstract

Self-assembled mixed-brushes with co-continuous surface morphologies were developed from melt of poly(ethylene glycol)-*b*-polystyrene (PEG-*b*-PS) and poly(ethylene glycol)-*b*-poly(methyl methacrylate) (PEG-*b*-PMMA) diblock copolymers by a self-seeding technique. Some features of solution-grown matrix-dispersed mixed-brushes having controllable characteristics were briefly recalled and compared with the behavior of corresponding melt-grown mixed-brushes. The preceding observations implied some major differences between two growth systems. An obvious deduction made from atomic force microscopy height images was that the patterned leopard-skin like surface morphology of solution induced mixed-brush single crystals changed to co-continuous morphologies in melt state. Beside the alteration of growth environment from solution to the melt, this phenomenon was assigned to the dominant kinetic effect replaced instead of the prevailed thermodynamic effect in dilute solution systems. The ratio of PMMA- to PS-covered surface area on the substrate, increased from 20/80 for the solution-grown mixed-brush single crystals to 50/50 for the melt-grown ones. Owing to

* Corresponding author

E-mail address: f.abbasi@sut.ac.ir

accelerated kinetic in melt-grown mixed-brush single crystals, for a same molecular weight, the thickness of a melt-grown mixed-brush single crystal was significantly greater than that observed for solution-grown mixed-brush single crystal. Similar trends, nevertheless, were observed for the thickness changes with molecular weight and crystallization temperature. The lateral sizes of melt-grown single crystals were about 4-fold larger than those for solution-grown single crystals (e.g., 24 vs. 6 μm). The thicknesses were also proved by the interface distribution function of small angle x-ray scattering analysis.

Keywords: self-assembled mixed-brush; co-continuous; PEG-*b*-PS; PEG-*b*-PMMA; melt-grown single crystals.

Introduction

Control of materials properties is one of the main purposes in the science realm. Some features, such as mechanical properties, are prone to regulation by the bulk structure or the composition of the materials. The biological responses are mostly tuned by the surface chemistry of materials, however. Surface modification is widely employed to adjust surface characteristics. There are several methods for successful alteration of surfaces, including mechanical methods, chemical coating and plasma etching [1-5].

Totally, polymer brushes are self-assembled polymer chains with one end grafted to the substrate. The chains extend away from the substrate, giving a longer end to end distance as they are in the freely random coiled conformation [6]. Successful modifications through polymer brushes, conducing to adhesive, protein-repulsive, hydrophobic and hydrophilic surfaces, have been reported [7-9]. To reach to combined properties in single grafted layer, a polymer mixed-brush is used, where two polymer chains with different features are tethered on a common

surface. Incorporating the second constituent significantly influences the brush's structure. Mixed-brushes are prepared by grafting to [10-14], grafting from [15-23], combination of both, and single crystal growth of star block copolymers [24-31]. Zhao applied atom transfer radical polymerization (ATRP) and then nitroxide-mediated radical polymerization (NMRP) to graft a polystyrene/poly(methyl methacrylate) (PS/PMMA) mixed brush [24]. Zhang *et al.* polymerized styrene and methyl methacrylate sequentially and obtained mixed-brushes on clay surfaces [32]. A new generation of mixed-brushes has been developed by single crystal surface patterning [33]. Recently single crystals have been utilized in the semiconductor microelectronics and solid-state science [34]. The PEO single crystals were also adopted as a simplified ultrathin film system to probe the interfacial properties of different substrates [35]. Our previous researches contributed to patterning of mixed-brushes and epitaxial structures of solution-grown single crystals [33,36]. In this work, we have changed the growth system from the dilute solution to the melt. The features of melt induced mixed-brushes drastically differed from corresponding samples in solution conditions. Lack of studies in this field inspired us for experimental research in melt state. A more detailed study led to a closer look at the mixed-brush single crystals developed from polymer melt and their differences with dilute solution-grown samples [33] which appear major. The new results mainly concern the behavior of melt-grown mixed-brush single crystals and the data are compared to and complement previous work, which is briefly recalled.

Experimental

Diblock copolymers were synthesized by ATRP according to the literatures [33,37]. ^{1}H NMR spectroscopy on a Bruker (Avance DPX) spectrometer, GPC on a Waters 1515 (USA) gel permeation chromatography instrument, and differential scanning calorimetry (DSC) (Netzsch,

F3 Maia) were adopted to analyze the characteristics of block copolymers. Molecular characteristics of PEG-*b*-PS and PEG-b-PMMA diblock copolymers are reported in Table S1. In this work, we utilized the self-seeding approach to prepare the mixed-brush single crystals from melt state which was described elsewhere [38-41]. The poly(ethylene glycol) (PEG)-*b*-PS and PEG-*b*-PMMA diblock copolymers were adopted in 50/50 weight of ratio. The homogeneous mixture of samples was put onto a cleaned silicon wafer under high purity nitrogen stream, and heated to above the melting temperature (T_m= 65 °C) and kept for about 30 min to obtain a homogeneous bulk layer. Afterward, it was switched to primary crystallization temperature (–10 °C) for 5-6 h. Then, it was transferred to the self-seeding temperature (T_s= 41 °C), and maintained for 30 min. The sample was then moved to a desired secondary crystallization temperature (T_c) and kept for 2-3 days. The characteristics of single crystals were investigated by DSC (Table S1), AFM, Nanoscope IIIA in the tapping mode, transmission electron microscope (TEM, EM 208 Philips) equipped with selected area electron diffraction (SAED) facility, and Bruker-AXS Nanostar SAXS with a counts rate of 1000 s/sec/channel and spatial resolution of 400-500 μm.

Results and discussion

In the past decades, it was thought that the melt-grown crystals were rarely single layer, once-folded, and ideal [42-44]; but our conducted experiments in this work elucidated that even in melt state, intervention of the polymer brushes can suppress extremely increase in thickness, multilayer structures, and screw dislocation reported in previous studies [45]. Similar to solution-grown systems [46,47], the population of ideal single crystals with grafted brushes on the surface was high in comparison to that in homopolymer single crystals (without any tethered chains on

the surface of the substrate). It is worth stating that based on the content of chains dispersed homogeneously on the silicon wafer, there existed some limitations in melt growth systems. More details are reported in Supplementary Information.

Co-continuous versus matrix-dispersed surface morphologies

In melt growth systems, the PMMA patches are connected together as if they were a unified phase region, whereas the PS-covered phase regions are homogeneous and continuous. *Thermodynamic effect* reflected in a matrix-dispersed surface morphology for solution-grown mixed-brush single crystals [33]. In melt-growth systems, in addition to thermodynamic effect, *kinetic effect* has an important influence on the surface morphologies. At the beginning of growth process from melt, the diblock copolymers of PEG-*b*-PS and PEG-*b*-PMMA are employed with the weight ratio of 50/50. Upon complete mixing of diblock copolymer chains the growth commenced. The possibility of presence of each type of crystallizable chains to attach to the growing seeds is to an extent the same; because the concentration of crystallizable chains and, consequently, the growth rate is high. However, despite the fact that in solution growth systems the weight ratio was 50/50 as well, due to low concentration and, consequently, the opportunity of thermodynamic selectivity, the chains attachments were based on their priorities [33].

In the melt state, the portion of PMMA chains has enhanced as compared to the solution state in amyl acetate at the same molecular weight and crystallization temperature. One of the reasons behind developing such morphologies could be ascribed to this fact that the PEG-*b*-PMMA chains with more compact conformation (due to more attraction to PEG block) would diffuse and reach easier to the growth region compared to more extended chains (PEG-*b*-PS).

Disregarding the interaction with the substrate, PMMA and PS brushes have similar radii of gyration (R_g) for the partly same molecular weights [48,49]. By drawing comparison between melt and solution states, we reached to some conceivable results. For PEG_{5000}-*b*-$PMMA_{8700}$/PEG_{5000}-*b*-PS_{14800} mixed-brush single crystal from melt at T_c= 30 ºC (Fig. 1(a)), though the gyration radius of PS chains is higher than PMMA ones, the thickness of substrate covered by PMMA brushes (even with significant lower molecular weight than PS ones) is less than PS-covered substrate thickness (9.08 nm vs. 10.21 nm). It declares that similar to solution-grown systems [37], in melt-grown mixed-brush single crystal system the attractive interaction of PMMA brushes with the substrate surface [49] has led to considerably higher osmotic pressure (a pressure exerted by a tethered chain on the surface of single crystal substrate to provide its required surface area to be expanded) for them in comparison with PS brushes. When the length of extended chain of PEG_{5000} (~27 nm [50]) is divided by crystalline substrate thickness in corresponding single crystal, the fold numbers can be calculated roughly. On the basis of the effective length, the fold numbers of PMMA- and PS-covered substrates are 3 and 2.6, respectively. The PEG_{5000}-*b*-$PMMA_{8700}$/PEG_{5000}-*b*-PS_{10000} mixed-brush single crystal at T_c= 30 °C is another sample, in which the osmotic pressure of PS chains is reduced for decreasing of M_n^{PS} and, subsequently for a lower required coverage surface area (the fold number of PS-covered substrate reached from 2.6 to 2.3); but the matrix-dispersed morphology is not appeared (Fig. 1(b)). The next system to compare is PEG_{5000}-*b*-$PMMA_{8700}$/PEG_{5000}-*b*-PS_{4600} mixed-brush single crystal at T_c= 30 °C. For higher R_g of PMMA chains and their attractive interaction with the substrate, the demanded surface area and, consequently, the osmotic pressure are higher for PMMA brushes compared to PS brushes. Simply, in previous mixed-brush single crystals (PEG_{5000}-*b*-$PMMA_{8700}$/PEG_{5000}-*b*-PS_{14800} and PEG_{5000}-*b*-$PMMA_{8700}$/PEG_{5000}-*b*-PS_{10000}), one of

parameters (greater R_g) was to the benefit of PS brushes and the other one (attractive interaction with the substrate) was to the advantage of PMMA brushes; but here (PEG_{5000}-*b*-$PMMA_{8700}$/PEG_{5000}-*b*-PS_{4600}), both hegemonies are with PMMA tethered chains. By comparing with former samples, here, the osmotic pressure of PS chains has decreased (the fold number of PS-covered substrate reached to 2.1) and, consequently, the difference of osmotic pressures of PS and PMMA brushes has elevated. So, the chance for matrix-dispersed surface morphology has increased. But anyway regarding the height images of AFM in Fig. 1(c), the surfaces have not yet taken matrix-dispersed morphology.

In the upcoming example, again the osmotic pressure of PMMA chains has increased and the difference between osmotic pressures of PS and PMMA is higher than previous example (PEG_{5000}-*b*-$PMMA_{8700}$/PEG_{5000}-*b*-PS_{4600}). This sample is PEG_{5000}-*b*-$PMMA_{17100}$/PEG_{5000}-*b*-PS_{4600} single crystal at T_c= 30 °C, in which the substrate thicknesses in PS- and PMMA-covered phase region are 12.79 and 8.02 nm, respectively. In these two samples with constant osmotic pressure of PS (for constant M_n^{PS}), the osmotic pressure of PMMA chains has raised for increase of M_n^{PMMA} and, consequently, increase of required coverage surface area. For single crystals of PEG_{5000}-*b*-$PMMA_{8700}$/PEG_{5000}-*b*-PS_{4600} (Fig. 1(c)) and PEG_{5000}-*b*-$PMMA_{17100}$/PEG_{5000}-*b*-PS_{4600} (Fig. 1(d)) the morphological behaviors were similar to each other. In fact, in PEG_{5000}-*b*-$PMMA_{17100}$/PEG_{5000}-*b*-PS_{4600} mixed-brush single crystals, the chance for getting matrix-dispersed surface morphology has been increased again; because the difference between osmotic pressures of two kinds of brushes (PS and PMMA) has enhanced. The fold number of PS- and PMMA-covered substrates is 2.1 and 3.4, respectively. Despite the fact that the osmotic pressures of PMMA and PS brushes are the highest and the lowest among the all grown single crystals, respectively, and respecting the extension of tethered chains, there is no trace of a

matrix-dispersed surface morphology (Fig. 1(d)). Therefore, in melt growth systems there exists another presiding parameter which is called kinetic effect.

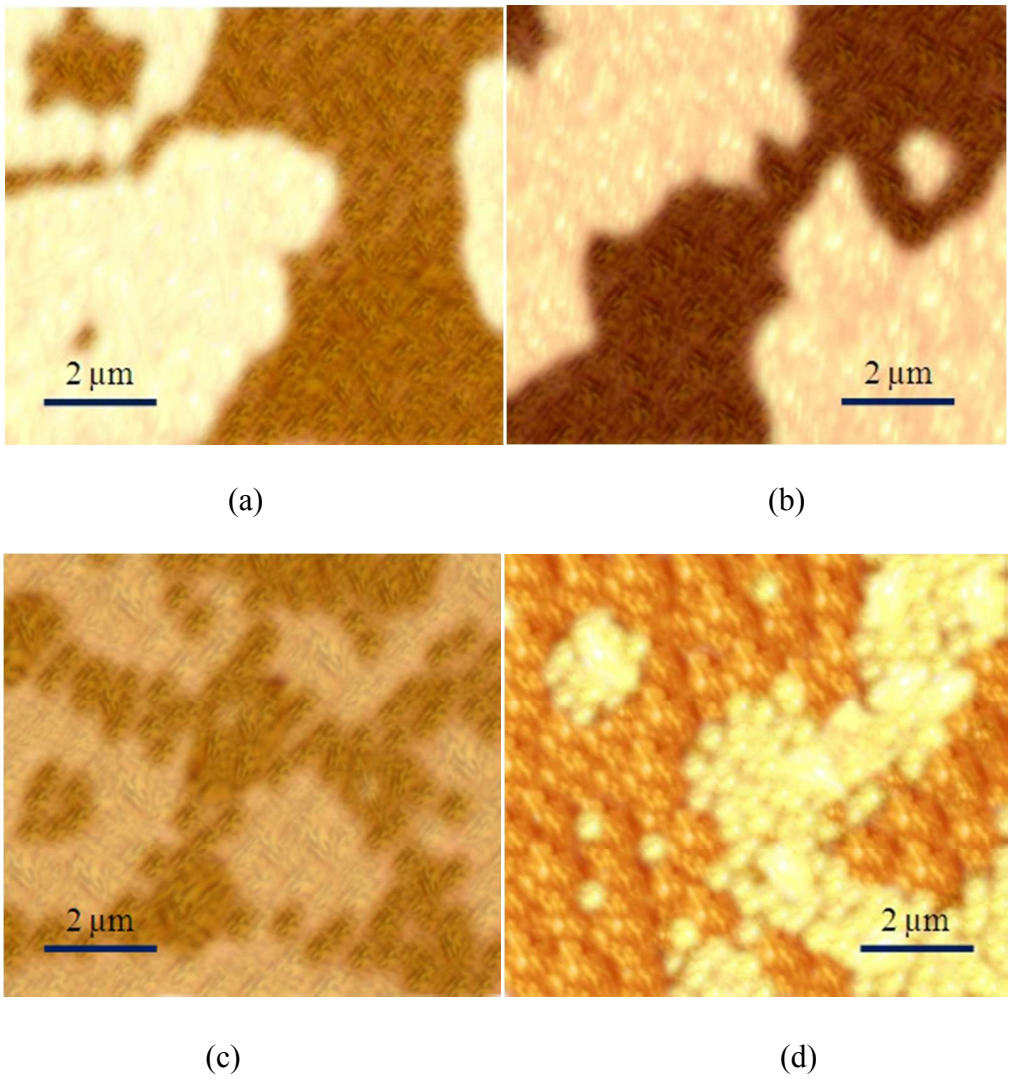

Fig. 1. The height images of mixed-brush single crystals at T_c= 30 °C for PEG_{5000}-*b*-$PMMA_{8700}$ (25.51 nm)/PEG_{5000}-*b*-PS_{14800} (45.84 nm) with height variance of 20.33 nm (a); PEG_{5000}-*b*-$PMMA_{8700}$ (25.54 nm)/PEG_{5000}-*b*-PS_{10000} (38.67 nm) with height variance of 13.13 nm (b); PEG_{5000}-*b*-$PMMA_{8700}$ (25.48 nm)/PEG_{5000}-*b*-PS_{4600} (26.69 nm) with height variance of 1.21 nm

(c); PEG_{5000}-*b*-$PMMA_{17100}$ (36.58 nm)/PEG_{5000}-*b*-PS_{4600} (26.67 nm) with height variance of 9.91 nm (d).

The mentioned examples indicate that the surface morphologies of melt-grown mixed-brush single crystals are completely distinct from those were grown from solution state (i.e., co-continuous vs. leopard-skin). In solution environment, amyl acetate (at 23-30 ºC) is a very good and a partially poor solvent for PS and PMMA chains, respectively [51,52]. On the contrary, in melt state both chains present in theta condition [53,54]. The theta condition for PS (compared to very good condition in solution system) causes PS chains to take packed conformation in comparison with very good solvent and thereby their hindrance is reduced against the PMMA chains. On the contrary, PMMA chains contain a higher extended conformation. Hence, their hindrance gets increased against the PS chains. On the other hand, PMMA brushes attract the substrate, and this could in turn not allow them to be extended. Here, from conformation perspective, the osmotic pressure of PS chains is on the fall whereas that of PMMA chains is to an extent on the rise as compared to solution state. Therefore, in addition to conformation, the osmotic pressure of contributing chains (PS and PMMA) approaches to each other. It may be thought that the difference between extension of tethered chains as well as osmotic pressure of PS and PMMA brushes has reduced due to being in the same kind of growth condition (theta condition). So, there is no possibility for getting matrix-dispersed surface morphology. In solution growth systems there were some samples in which the substrate height variances were very low. As an instances, in PEG_{5000}-*b*-$PMMA_{17100}$/PEG_{5000}-*b*-PS_{14800} mixed-brush single crystal at T_c= 23 ºC, the substrate thicknesses of PS- and PMMA-covered phase regions were equal to 4.0 and 2.7 nm, respectively. In this sample the substrate height variance was 1.3 nm

(48% of lower thickness and 32.5% of higher thickness). In PEG_{5000}-*b*-$PMMA_{17100}$/PEG_{5000}-*b*-PS_{4600} single crystal grown from melt state (the highest osmotic pressure difference between PMMA and PS brushes) at T_c= 23 ºC (10.95 nm for the thickness of PS-covered substrate and 6.91 nm for that of PMMA-covered substrate) the substrate height variance is 4.04 nm (~ 58.5% of lower thickness and ~ 37 of higher thickness). Indeed, the difference of osmotic pressure in PEG_{5000}-*b*-$PMMA_{17100}$/PEG_{5000}-*b*-PS_{4600} at T_c= 23 ºC grown from melt is high compared to that in PEG_{5000}-*b*-$PMMA_{17100}$/PEG_{5000}-*b*-PS_{14800} at T_c= 23 ºC grown from dilute solution. Even though the osmotic pressure of PMMA brushes is higher, they are not allowed to be dispersed in the PS-matrix. Beside the osmotic pressure, the extension of tethered chains (PS and PMMA) is another parameter which could have effect on the surface morphology. In theta condition of melt state the conformations of PS and PMMA chains approach to each other. So, their tendency to attract the opposite type of chains increases. This could in turn conduce to co-continuous surface morphologies.

In addition, in theta solution system at T_c= 23 ºC, the decrease of substrate thickness from homo-PEG_{5000} (10.33 nm) to PEG_{5000}-*b*-PS_{4600} (6.50 nm) single crystal with the lowest osmotic pressure was 37%. This reduction is for entropic effect of tethered chains on the substrate. However, in melt system at the same crystallization temperature and for the same samples the decrease of substrate thickness was 18.5% (from 13.51 nm to 11.00 nm). Due to higher thickness of pristine single crystal (homo-PEG_{5000}), and without considering the kinetic effect, this decrease must have been larger; because for the same decrease in the substrate thickness the tethered chains will have a more enlarged compactness in the vicinity of each other in comparison with corresponding solution-grown sample. So, to suppress this higher compactness of amorphous brushes (to have lower entropy enhancement for compactness of brushes), the

substrate thickness has to undergo a greater decrease. Actually, here, the kinetic effect does not let the crystalline chains have more fold numbers. Therefore, the substrate thickness and, consequently, the amorphous brushes and total thickness are more enlarged than corresponding solution growth environment. Likewise, at T_c= 23 ºC in theta solution-grown single crystals of homo-PEG_{5000} and PEG_{5000}-*b*-$PMMA_{17100}$ (having the highest osmotic pressure), the substrate thickness variance was 74% (from 10.33 nm to 2.70 nm). In respective melt-grown single crystals at the same crystallization temperature, the substrate thickness variance was 49.5% (from 13.51 nm to 6.83 nm), however. Here, the mentioned kinetic effect satisfies the condition as well. The kinetic effect contributes to a high concentration of crystallizable chains, the accessibility of polymer chains in growth system and, consequently, a high growth rate in polymer melt state.

Surface morphologies developed from PEG-*b*-PS and PEG-*b*-PMMA chains in bulk state are randomly distributed. This phenomenon can also be resulted from kinetic effect, otherwise like solution-grown mixed-brush single crystals having regular leopard skin surfaces it must have possessed a common surface morphology. It is interesting that the total, substrate and brush thicknesses in PS- and PMMA-covered phase regions, for a given molecular weight, in all parts of a sample and even in different samples with distinct surface morphologies are consistent with each other. AFM height profiles proved our claims. This phenomenon resembled the solution systems.

Characteristics and Trends

On the basis of Hoffmann-Lauritzen theory [55], the crystal thickness is thermodynamically determined by the surface energy, γ_e. The d_{CRYST} of a homopolymer single crystal is proportional

to the reciprocal undercooling, $1/\Delta T$, and follows a linear relationship with $1/\Delta T$ (Eq. (1)) [51,55-57]:

$$d_{CRYST} = \frac{2\gamma_e T_d}{\Delta h_d \Delta T} = \frac{2\gamma_e T_d}{\Delta h_d (T_d - T_c)} \quad (1)$$

where T_d is the equilibrium dissolution temperature, γ_e is the fold-surface free energy, and Δh_d is the equilibrium heat of dissolution.

In the homopolymer case, γ_e is defined by the fold-surface free energy, γ_c; however, in diblock copolymer single crystals, an additional term, γ_t, or the free-energy contribution from the tethered chains, must be brought into consideration (i.e., $\gamma_e = \gamma_c + \gamma_t$). γ_t is related to the tethering density and conformation of the tethered amorphous chains. Up to now, it is thought that the amorphous blocks can affect the crystallization through changing the free energy. Here, we introduce another effective parameter, i.e., kinetic effect.

In this work, totally, the brushes fabricated from melt-grown single crystals are embedded in higher regimes than those in solution-grown mixed-brush single crystals [33]. More details based on the reduced tethering densities ($\tilde{\sigma}$) [51,58,59] are reported in Supplementary Information. In highly compacted regimes, the effect of tethered chains is more dominant on substrate thickness. In our growth systems, despite the fact that melt fabricated brushes are in more compact regimes, the respective substrate thicknesses are thicker. Hence, the considerable increase in substrate thicknesses could not be due to dominant effect of enthalpy to entropy, which is an acceptable theory to determine the substrate thickness in single crystals to date. This theory states that thermodynamically, the final crystal morphology of PEO diblock copolymers reflects the balance between an enthalpic driving force to minimize the fold-surface energy and the entropic term resulting from stretching of amorphous blocks [60]. In the melt state, the concentration is higher and, subsequently, the growth rate is higher. So, the crystallizable chains do not have enough

time to get more folds. Therefore, they construct substrates with larger thicknesses. In conclusion, in melt systems the kinetic effect prevails the growth condition. It was demonstrated that extremely high regimes for tethered chains on the substrate do not allow the respective single crystals to be developed [46].

By comparing theta solvent and melt state, similar results were obtained. As an instance at T_c= 23 °C for PS_{4600}-covered phase regions, $\tilde{\sigma}$ values were 11.37 and 7.33 in melt state and theta solvent, respectively.

Although in solution and melt growth systems of mixed-brush single crystals the thicknesses are completely different (i.e., the total and substrate thicknesses are greater in melt state) the trends of thickness change with crystallization temperature and molecular weight are similar for both systems. When a crystallizable chain attaches to a growing seed in melt state and tends to fold, presence of other chains in its vicinity (in a big population) does not allow that to have thermodynamic dictated folds. Hence, lower folding results in more enlarged substrate thickness. Subsequently, when the substrate has lower folding the grafted amorphous chains are closer to each other on the surface of single crystal, and this would in turn more heighten the brushes. Figs. 2(a) and (b) display the increasing trends of total and substrate thickness vs. crystallization temperature, respectively. In melt state, the slopes of graphs of total and substrate thicknesses vs. crystallization temperature are steeper for both PS- and PMMA-covered regions. This steeper slope could be indicating an accelerated kinetic in melt-grown single crystals. In details, in melt state the thicknesses of substrates are greater; so, the compactness of tethered chains is higher, i.e., the brushes are in the higher regimes compared to solution state. Hence, by increasing the crystallization temperature, the escalating of substrate thickness will be more hampered in comparison to solution state. But the graphs of Fig. 2(b) depict that the situation has happened

reversely, and the slope of substrate thickness as well as overall height vs. crystallization temperature variations is steeper for melt grown samples. Here, this is the kinetic effect which causes the slope of thickness variances vs. crystallization temperature to be steeper than solution systems through partially frustration of the tethered amorphous chains.

Although the radius of gyration (R_g) of PS brushes with M_n= 14,800 g/mol is drastically higher than R_g of PMMA brushes having M_n= 8,700 g/mol, as an instance at T_c= 23 ºC the thickness of PMMA-covered regions was lower than PS-covered regions (3.5 nm vs. 4.0 nm) [33]. On the basis of this fact we concluded that due to attractive interaction of PMMA brushes with substrate, their osmotic pressure was higher and, consequently the respective substrate thickness was lower as well (even in the lowest molecular weight of PMMA brushes).

The total thickness of grown single crystals is obtainable from AFM height profiles. The crystalline substrate thickness (d_{CRYST}) can be determined from Eq. (2) [51,61].

$$d_{CRYST} = d^{total} \times \frac{M_n^{CRYST}/\rho_{CRYST}}{M_n^{CRYST}/\rho_{CRYST}+M_n^{AM}/\rho_{AM}} \quad (2)$$

where ρ_{CRYST}, d_{CRYST}, ${M_n}^{CRYST}$, d^{total}, M_n^{AM}, and ρ_{AM} stand for the crystalline PEG density (=1.239 g/cm^3 at room temperature) [62], PEG substrate thickness, the molecular weight of PEG (5,000 g/mol), the total thickness, the molecular weight of amorphous blocks, the density of amorphous blocks (1.19 g/cm^3 for PMMA [52] and 1.05 g/cm^3 for PS [63]), respectively.

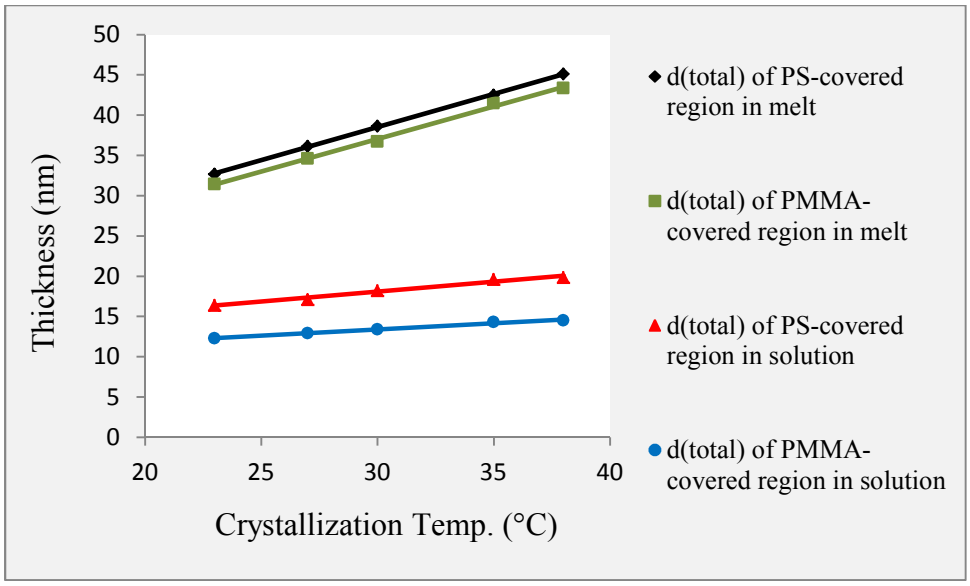

(a)

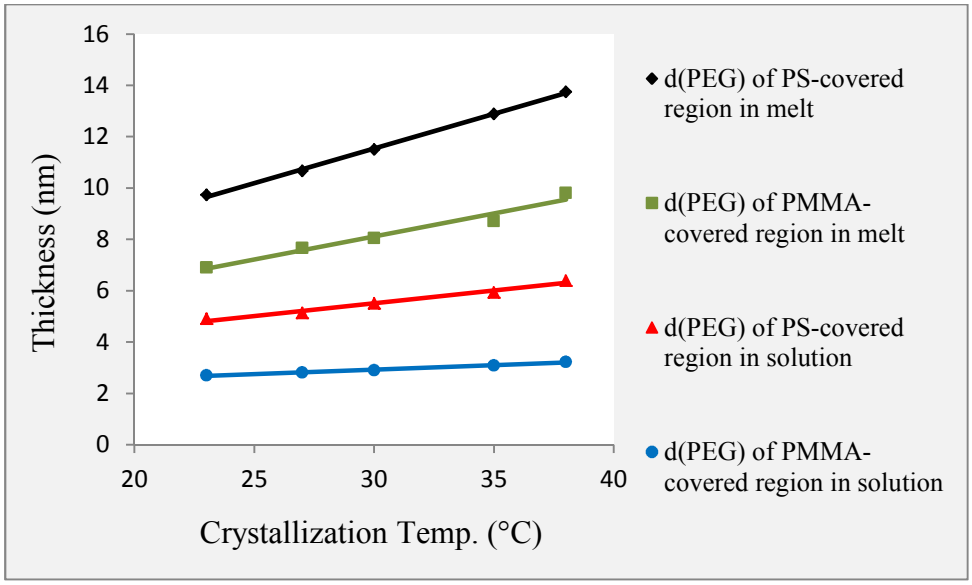

(b)

Fig. 2. Variations of single crystals thicknesses having mixed-brush surface morphologies grown from solution and melt states vs. crystallization temperature for PEG_{5000}-*b*-$PMMA_{17100}$/PEG_{5000}-*b*-PS_{10000}; total thicknesses (a); substrate thickness (b).

Resembling solution growth systems, in melt-grown mixed-brush single crystals the features of each phase region affected only its own thickness. More details with elucidating examples are rendered in Supplementary Information.

The thermodynamic parameters including the solvent type, molecular weight, interaction with substrate, and temperature exist in both dilute solution and melt state. In solution growth systems the thickness is mainly affected by osmotic pressure of grafted chains which is determined by their interaction with solvent and respective substrate. The domain sizes of PMMA-patches were also completely controllable in PS-matrix phase. Here, we discuss on some detailed influences of kinetic effect in melt condition based on the graphs of Figs. 3(a)-(d).

By altering the growth condition from solution to melt, the substrate thickness enhancement for both PS and PMMA brushes is the same (Figs. 3(a) and (b)). For PEG_{5000}-*b*-$PMMA_{13100}$/PEG_{5000}-*b*-PS_{4600} at T_c= 23 ºC, d_{PEG} for PMMA-covered regions reaches from 3.00 nm in solution to 7.16 nm in melt (Fig. 3(a)). Likewise, d_{PEG} for PS-covered regions changes from 6.8 nm in solution to 10.96 nm in melt, and for both substrates the height difference is 4.16 nm (Fig. 3(b)). The PMMA brushes get an expanded conformation from poor solvent to theta state. This causes the brushes to exert a higher osmotic pressure on the substrate. On the other hand, the PS brushes are transferred from very good solvent to melt theta condition. So, they should get a more compact conformation. In the mentioned sample (PEG_{5000}-*b*-$PMMA_{13100}$/PEG_{5000}-*b*-PS_{4600}), M_n^{PMMA} is greater than M_n^{PS} and PMMA brushes have attractive interaction with the PEG substrate [33]. All these effects would not allow PS- and PMMA-covered substrates to heighten thickness at the same level. So, PMMA-covered phase regions in the structure of mixed-brush single crystals more benefit from kinetic effect to increase their substrate thickness. Simply, the chains with higher hindrance to impede increase of the substrate

thickness in solution state share a greater contribution in kinetic dominant growth condition and when the growth condition changes from solution to melt highly escalate their substrate compared to the chains with lower hindrance. Regardless of substrate effect, although in solution state PMMA and PS brushes were in partially poor and very good solvents, respectively, the height of PMMA chains was more enlarged than PS chains. Here in melt state, PMMA chains are in the theta condition and have more expanded conformation. This in turn increases the height variance of two kinds of brushes. On the other hand, the growth condition of PS chains is changed from very good to theta. So, they have gotten a smaller conformation. This also enhances the respective amorphous height variance. Actually, when the thickness of PS- and PMMA-covered substrates increases at the same level, PMMA brushes are more heightened in melt state. The amorphous height variance of –3.83 nm for melt in comparison with –0.4 nm for solution proves this fact. In addition to the effect of brushes conformation, highly escalated PMMA-covered substrate compared to PS-covered substrate from solution to melt reflects in more compressed brushes. In fact, the kinetic has highly suppressed PMMA chains thermodynamics in comparison to PS chains. Based on rendered explanations the primary difference of PS and PMMA brushes in melt state (= –3.83 nm) is greater than that in solution state (= –0.4 nm).

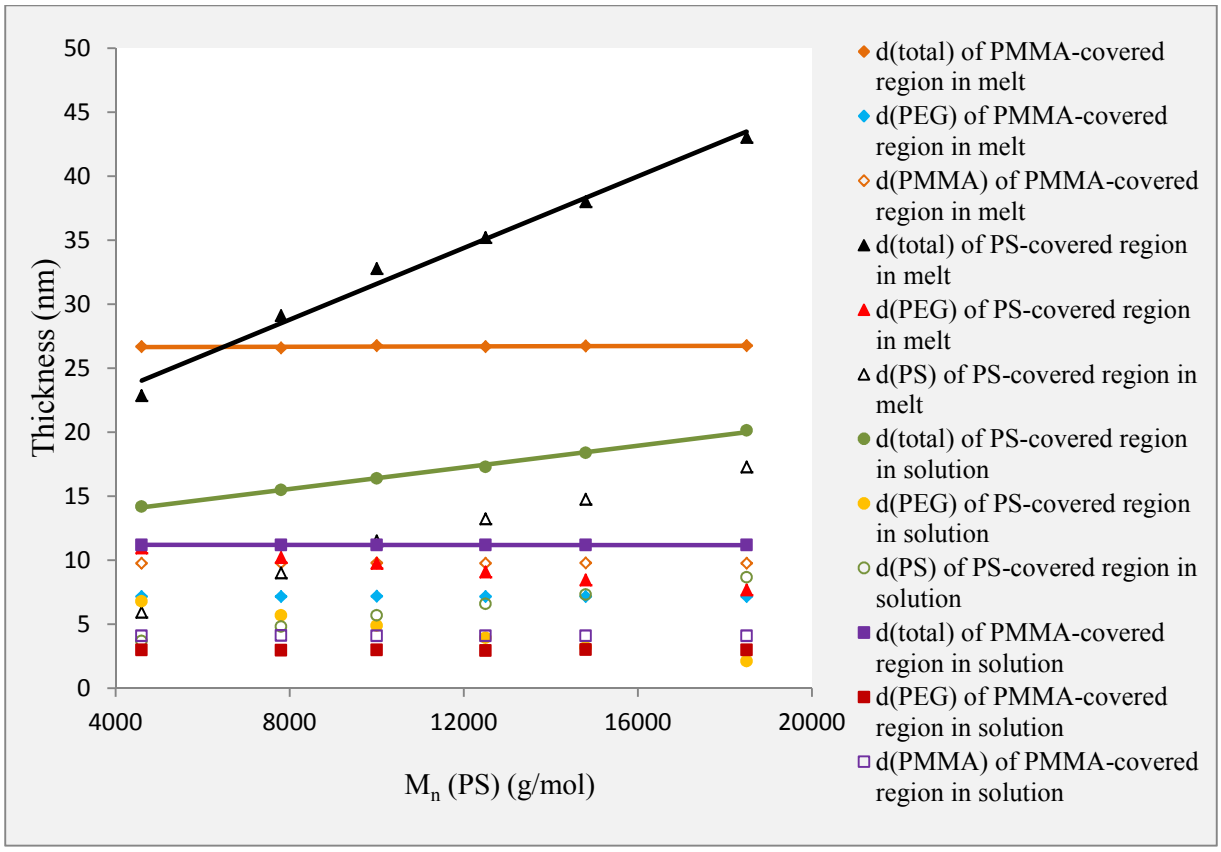

(a)

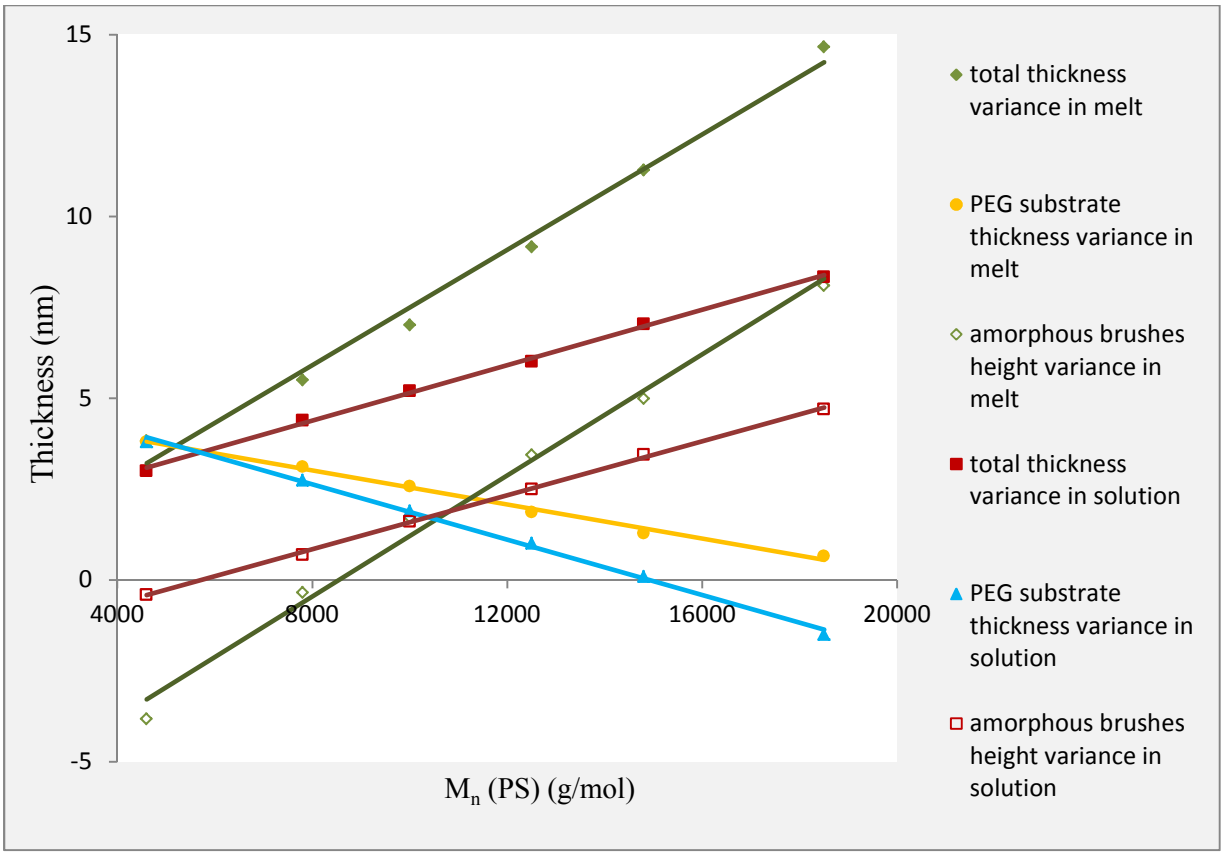

(b)

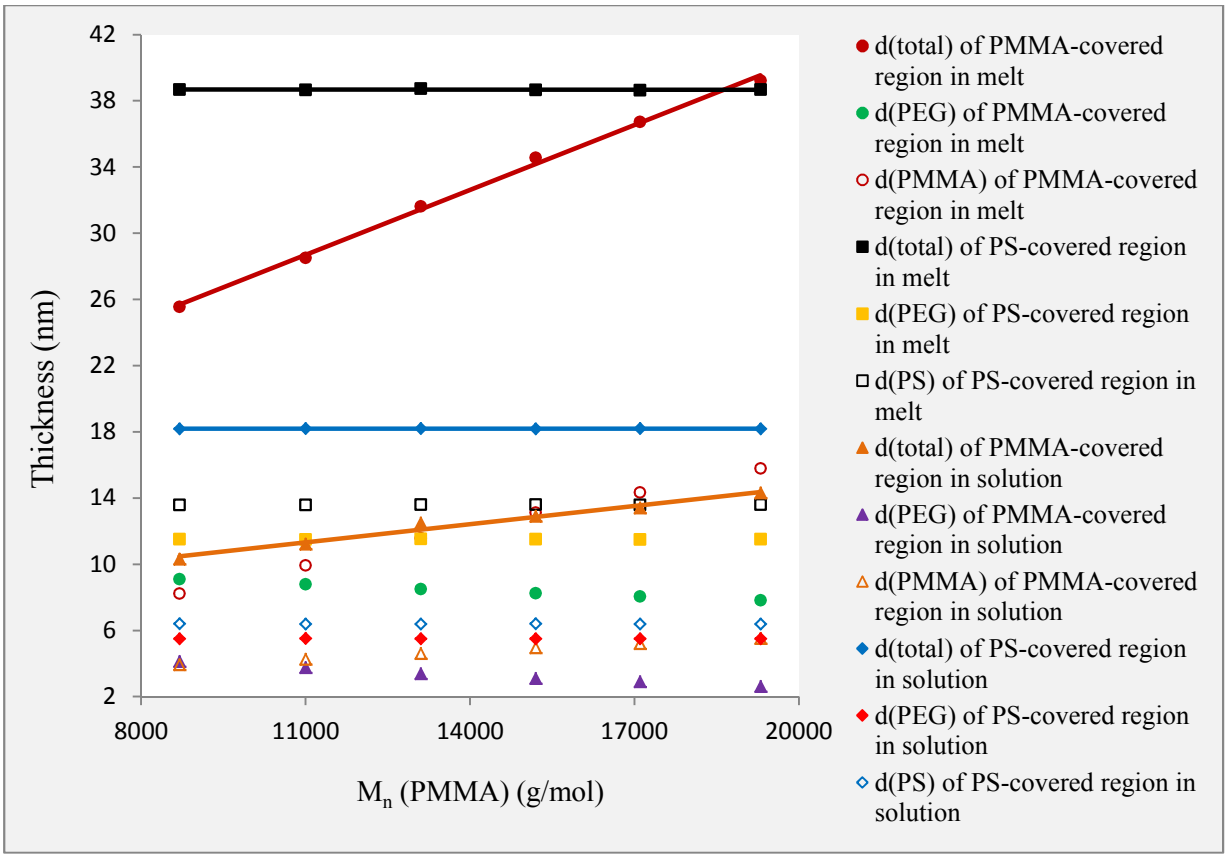

(c)

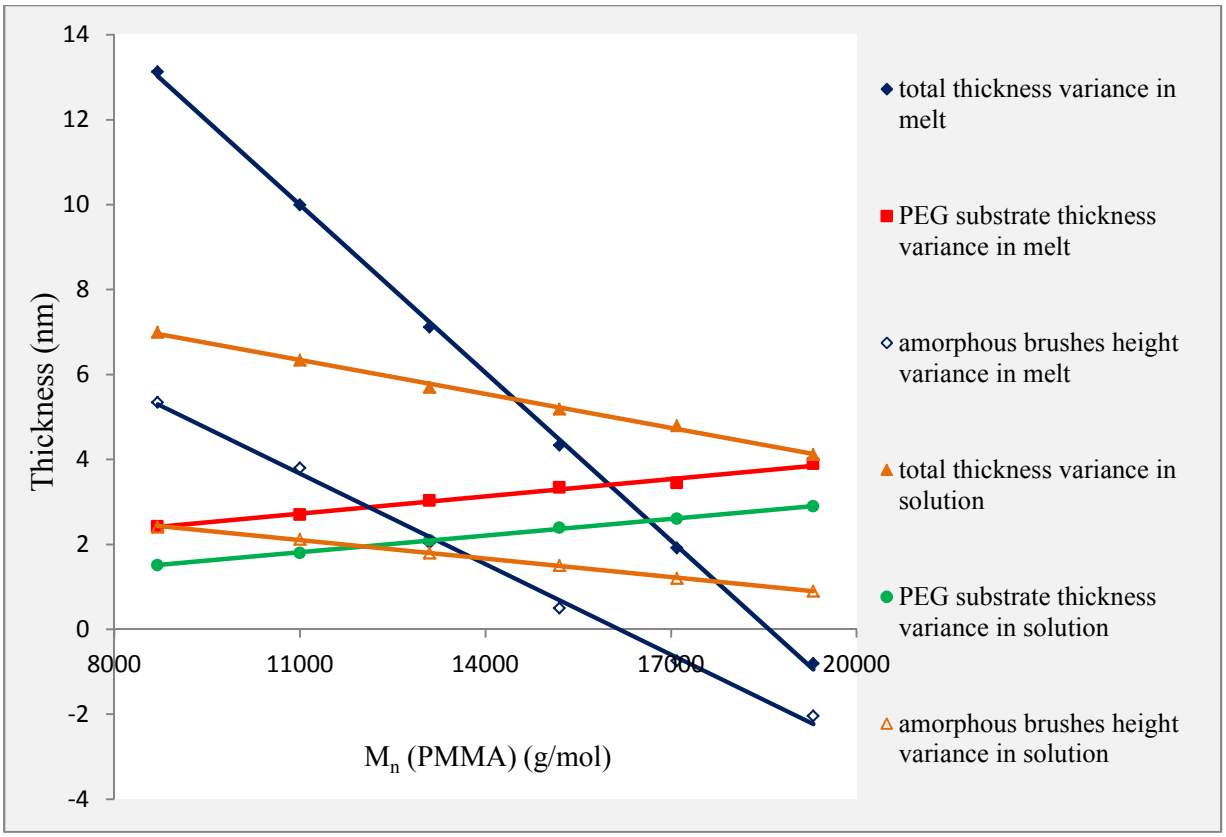

(d)

Fig. 3. The thicknesses (a and c) and height variances (b and d) vs. molecular weight. In the graphs of (a) and (b) M_n^{PMMA} is 13,100 g/mol and the molecular weight of PS brushes enhances gradually at T_c= 23 ºC; in the graphs of (c) and (d) M_n^{PS} is 10,000 g/mol and the molecular weight of PMMA brushes increases gradually at T_c= 30 ºC. The differences are obtained by the characteristics of PS brushes minus PMMA ones.

Besides, the higher hindrance of increase of M_n^{PS} and kinetic induced hindrance are two reasons for steeper slope of amorphous height variance in melt state. In details, although the conformation of PS chains is more compact in comparison to good solvent, they are in higher regimes in melt state. It could be attributed to the greater substrate thickness of melt-grown single crystals. Hence, in melt by increasing M_n^{PS}, PS brushes insert a higher force to each other

(in comparison to the corresponding sample grown from solution) and, consequently, are more extended. Therefore, the approach of PS brushes height to that of PMMA chains is more accelerated (i.e., the graph is steeper (Fig. 3(b)). Another reason for steeper amorphous height variance graph vs. M_n^{PS} is that when M_n^{PS} increases from 10,000 to 14,800 g/mol, once again the hindrance of PS brushes enhances. So, here the kinetic further affects the substrate and, consequently, PS chains are more extended (in comparison to corresponding variances from 4,600 to 10,000 g/mol).

Now, we draw comparison between the slopes of graphs of substrate height variances between solution and melt states. In melt state, although PS brushes are in a more compressed condition, due to kinetic effect they do not have opportunity to exert their thermodynamic dictated osmotic pressure. So, they are not capable to force PS-covered substrate to approach to PMMA-covered substrate compared to PS brushes with lower molecular weights. In conclusion, due to dominant kinetic effect in melt-grown condition, by increasing M_n^{PS} the variance between the substrate thicknesses of PS- and PMMA- covered regions for melt state is lower than solution, and the slope of respective graph for melt is less than that of solution (Fig. 3(b)).

Finally, the slope of total height variance in melt is steeper than solution; because the slope of heightening of brushes is bigger than the slope of decrease of substrate thicknesses.

In Fig. 3(c) for PEG_{5000}-*b*-$PMMA_{13100}$/PEG_{5000}-*b*-PS_{10000} the pristine thickness of PS brushes (= 6.4 nm) is more enlarged than PMMA brushes (= 4.6 nm) in solution. So, when the single crystal is grown from melt, the kinetic effect only neutralize the attractive interaction of PMMA chains with the substrate as well as their more expanded conformation (from solution to melt), while in PEG_{5000}-*b*-$PMMA_{13100}$/PEG_{5000}-*b*-PS_{4600} (Fig. 3(b) with negative amorphous height variance which means that the height of PMMA chains is greater than that of PS ones) the kinetic also

reciprocate the higher height of PMMA brushes. Indeed, here due to higher pristine height of PS chains than PMMA ones in solution state, the kinetic is to neutralize this hindrance. Therefore, for PEG_{5000}-*b*-$PMMA_{13100}$/PEG_{5000}-*b*-PS_{10000} mixed-brushes in comparison to PEG_{5000}-*b*-$PMMA_{13100}$/PEG_{5000}-*b*-PS_{4600}, the substrate of PS-covered area has a higher elevation compared to PMMA-covered regions in moving from solution to melt. This causes a greater substrate thickness variance for PEG_{5000}-*b*-$PMMA_{13100}$/PEG_{5000}-*b*-PS_{10000} sample in solution and melt states. The graphs of substrate thickness variances are parallel for solution and melt conditions (Fig. 3(d)). When M_n^{PS} is 10,000 g/mol, by increasing M_n^{PMMA} from 13,100 to 17,100 g/mol, first, due to more enlarged pristine thickness of PMMA-covered substrate (for kinetic effect) and second, for more expanded conformation of PMMA chains (from poor to theta condition), PMMA brushes are embedded in higher regimes. So, the respective hindrance is greater and, consequently, the kinetic more affects and substrate thickness is much more elevated than before. In fact, if the kinetic effect did not intervene, through passing from 13,100 to 17,100 g/mol, the substrate thickness must have highly decreased and the substrate thickness variance must have more increased. Anyway, in melt the kinetic has highly neutralized the higher hindrance of PMMA brushes having M_n^{PMMA}= 17,100 g/mol, and consequently, has further elevated the substrate.

In Fig. 3(d) PS brushes are always thicker than PMMA ones but in melt sometimes PMMA brushes overtake from them. Here, the hindrance of PMMA chains is greater. So, the kinetic more affects them and keeps the substrate thickness of PMMA-covered regions higher than that of PS chains. As a result, PMMA chains get more compresses. On the other hand, PMMA chains are transferred from poor to theta condition and the chains are larger whereas PS chains are

moved from very good to theta condition. Therefore, PMMA brushes have a better opportunity to overtake from PS ones height wise in melt state.

Eventually, the reason of steeper graphs of PS and PMMA brushes height variance in melt state when M_n^{PS} is 10,000 g/mol and M_n^{PMMA} changes from 13,100 to 17,100 g/mol could be attributed to some features. First, PMMA chains condition is altered and, subsequently, they are more stretched. Second, due to kinetic effect the pristine thickness of PEG substrate in melt is larger than that in solution. Therefore, the brushes exert higher force to each other and, consequently, are highly heightened. Third, in melt state the kinetic do not let the substrates have their thermodynamic based thickness, and keeps the substrates in larger thicknesses. So, the brushes are more compressed to each other and, consequently, get more elevation. This could cause PMMA brushes to approach to the height of PS ones with higher acceleration (i.e., bigger slope) in comparison to the similar situation in solution state.

The ratio of PMMA-covered to PS-covered surface areas on the substrate surface of mixed-brush single crystals was determined by Image J software of AFM. Totally, the ratio of PMMA to PS brushes was somehow 20/80. In polymer melt-grown corresponding mixed-brush single crystals this ratio altered to 50/50. The graphs (a) and (b) in Fig. 4 depict these ratios. As explained previously, the extension of tethered PS and PMMA chains could be an effective parameter on the surface morphology. In theta condition of melt state the conformations of PS and PMMA chains approach to each other and, consequently, the system's tendency to attract the opposite type of chains increases. Hence, this could in turn lead to co-continuous surface morphologies with higher portion for PMMA brushes.

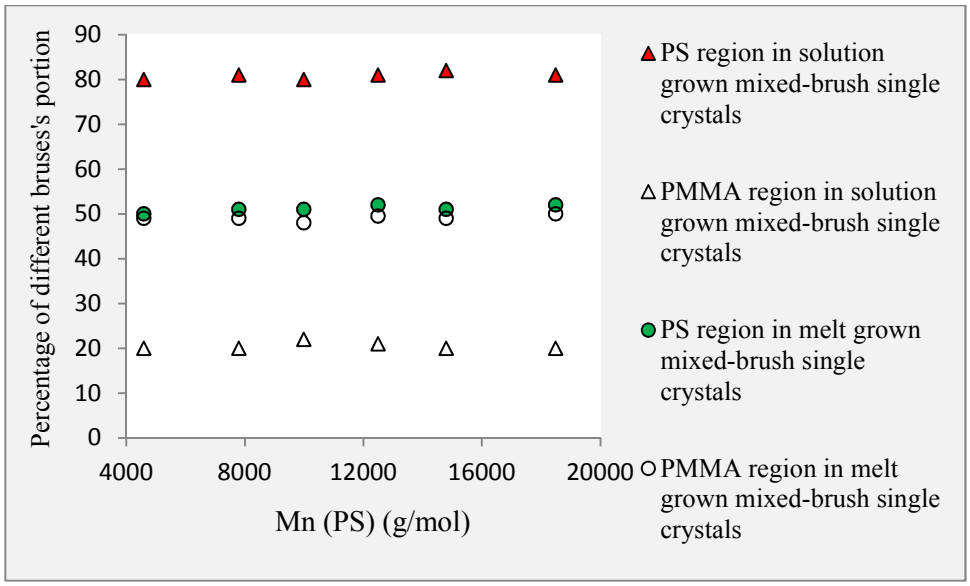

(a)

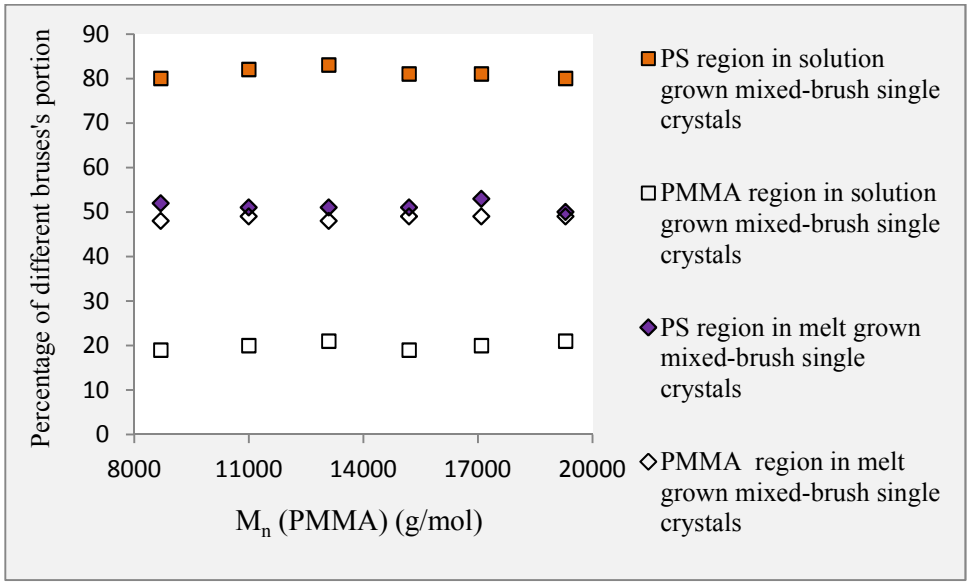

(b)

Fig. 4. The percentage of each of PS and PMMA polymer brushes. (a) M_n^{PMMA}= 17,100 g/mol and the molecular weight of PS brush increases; (b) M_n^{PS}= 4,600 g/mol and the molecular weight of PMMA brush increases.

Another significant difference between crystals grown in solution and from melt is the orientation of the four other growth faces. On the contrary of grown single crystals from a dilute solution, in which the overall lateral habits were square or truncated square with (120), (110) and (020) prisms [33], in melt state the general shapes are hexagonal. Here in melt-grown mixed-brush single crystals from PEG-*b*-PS and PEG-*b*-PMMA polymer chains, when (140) fronts are predominant the lateral habit is square (Fig. 5) as well whereas when (100) growth faces appear in electron diffraction (ED) patterns the overall shape turns to hexagonal habit (Fig. 5).

In some rare cases, in some parts of melt-grown single crystal surface like in solution, the matrix-dispersed morphology has been developed. In these samples, the PMMA-covered phases are dispersed in PS-matrix (Fig. 5). In hexagonal shaped, solution-grown crystals, these faces are parallel to the (120) planes [39], whereas in melt-grown crystals they correspond (and are often tangential) to (140) planes [64]. In melt-grown crystals the pair of truncating prism faces are parallel to the (100) planes instead of being normal to them as in solution-grown crystals [39].

Some details of the micro-structure of the two-phase system can be analyzed using the interface distribution function (IDF) developed by Ruland [65]. The IDF ($g_1(r)$) (Eq. (3)) provides a series of the distance distributions with alternating signs.

$$g_1(r) = \frac{\partial^2(\gamma_1(r))}{\partial r^2} = \gamma_1{}''(r) \qquad (3)$$

$\gamma_1(r)$ is 1D correlation function. As shown by Stribeck and Ruland [66] from the analysis of this function one can obtain LB (the total thickness of single crystal), L_c (crystalline substrate thickness), L_a (the twice of amorphous brushes thickness) and the width of the corresponding distribution. In addition to utilize the AFM and respective relations for calculating the substrate and amorphous brushes thickness, we applied SAXS to verify the calculated thicknesses, whereas in solution-grown single crystals we developed epitaxial structures to do this

verification [36]. In respective graph of IDF for homopolymer single crystals, which is plotted vs. *r* (nm), the first valley is LB, and the two positive peaks (depending on the molecular weight of crystalline and amorphous blocks) depict L_a and L_c or vice versa [67]. Here, for mixed-brush single crystals there are two distinct crystalline substrate thicknesses and two various amorphous brushes. In IDF of Fig. 6 for PEG_{5000}-*b*-$PMMA_{17100}$/PEG_{5000}-*b*-PS_{4600} mixed-brush single crystals, two first peaks stand for the substrate thickness of PMMA-covered (= 8.15 nm) and PS-covered (=12.55 nm) phase regions, respectively. Likewise, two second peaks are representatives of twice of amorphous brushes thickness of PS (= 13.98 nm) and PMMA (= 28.70 nm).

Figs. 5 and 6 depict the analytical features of PEG_{5000}-*b*-$PMMA_{17100}$/PEG_{5000}-*b*-PS_{4600} mixed-brush single crystal in the frame of height image and height profile of AFM and SAXS graphs.

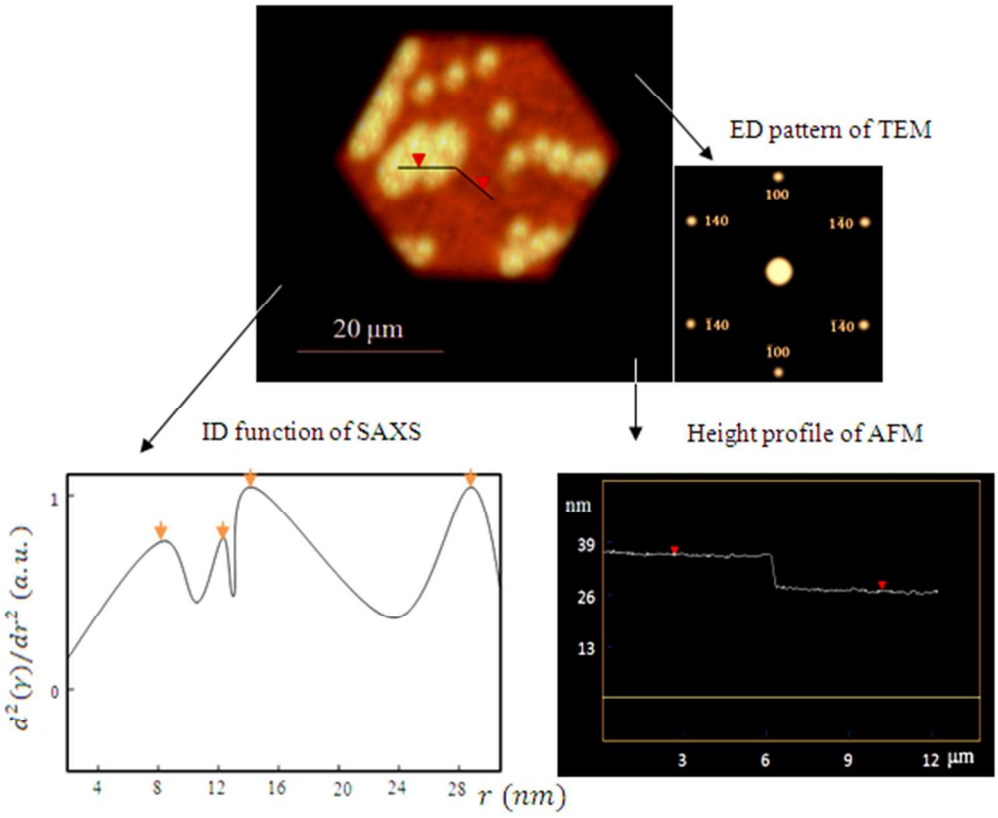

Fig. 5. The features (AFM height image, electron diffraction (ED) patterns of TEM, height profile of AFM and SAXS graph) of PEG_{5000}-*b*-$PMMA_{17100}$ (36.58 nm)/PEG_{5000}-*b*-PS_{4600} (26.67 nm) melt-grown mixed-brush single crystals at T_c= 30 ºC with height variance of 9.91 nm.

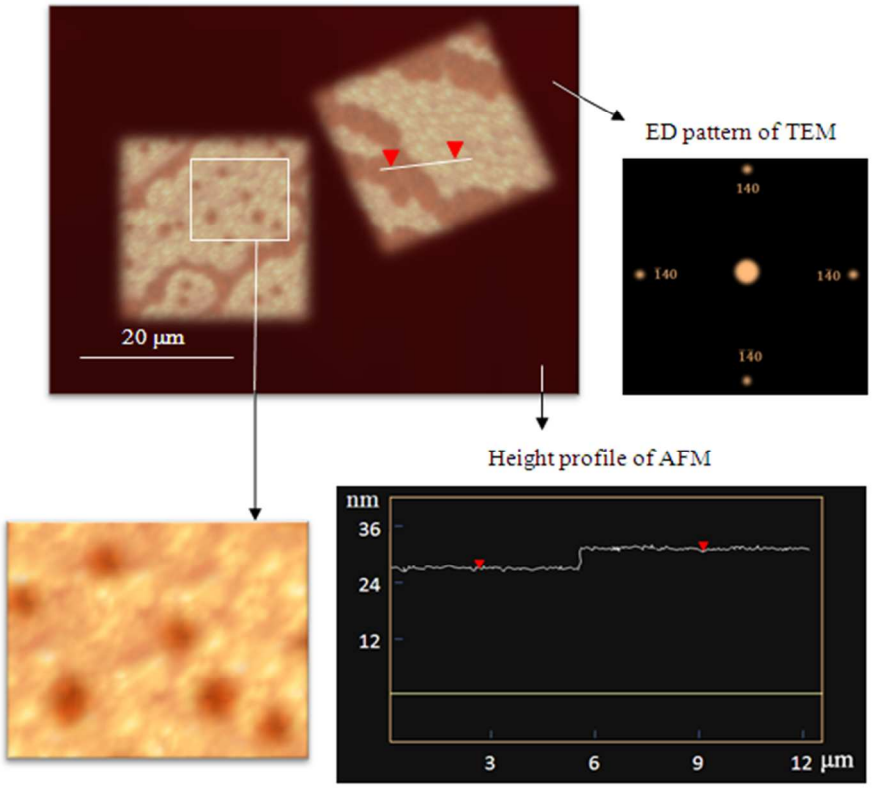

Fig. 6. The features (AFM height image, electron diffraction (ED) patterns of TEM, height profile of AFM and zoomed surface morphology) of PEG_{5000}-*b*-$PMMA_{13100}$ (26.77 nm)/PEG_{5000}-*b*-PS_{10000} (32.79 nm) at T_c= 23 ºC melt-grown mixed-brush single crystals with height variance of 6.02 nm.

In theta solvent the chains take a shape and conformation as if they present in their bulk state. The slope of total thickness vs. M_n^{PS} for PEG-*b*-PS single crystals grown from melt is considerably higher than that of grown from theta solvent. The total and amorphous brushes

thicknesses on the single crystal substrate for melt are also significantly higher than corresponding thicknesses in theta solvent. In melt state the polymer chains are more available, and this could in turn help an accelerated kinetic. However, in dilute solution growth condition the chains are far away from each other. This enough space allows the solvent and interaction with substrate effects to be more effective. Fig. 7(a) and (b) draw comparison between characteristics of PS-covered phase regions in theta solvent and melt state vs. M_n^{PS} and crystallization temperature, respectively.

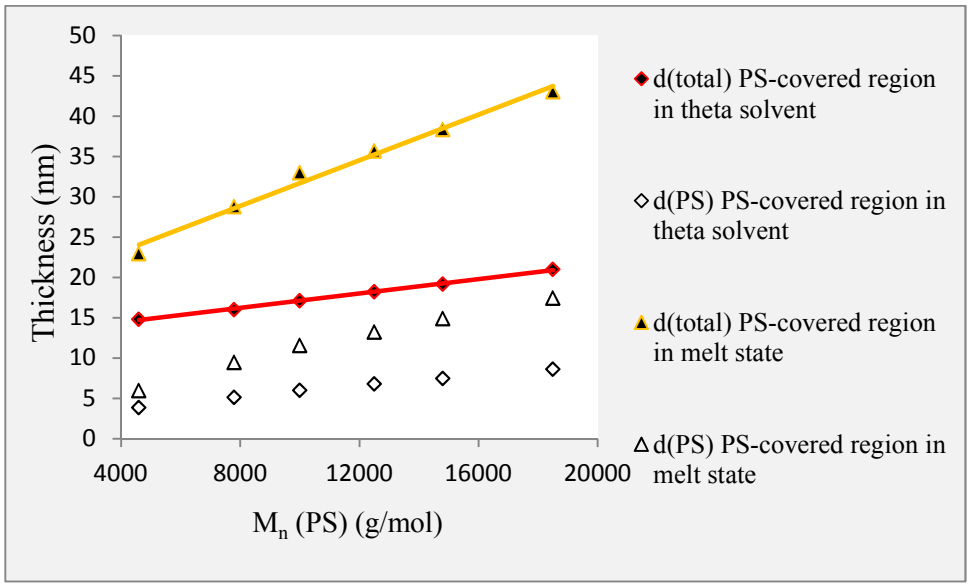

(a)

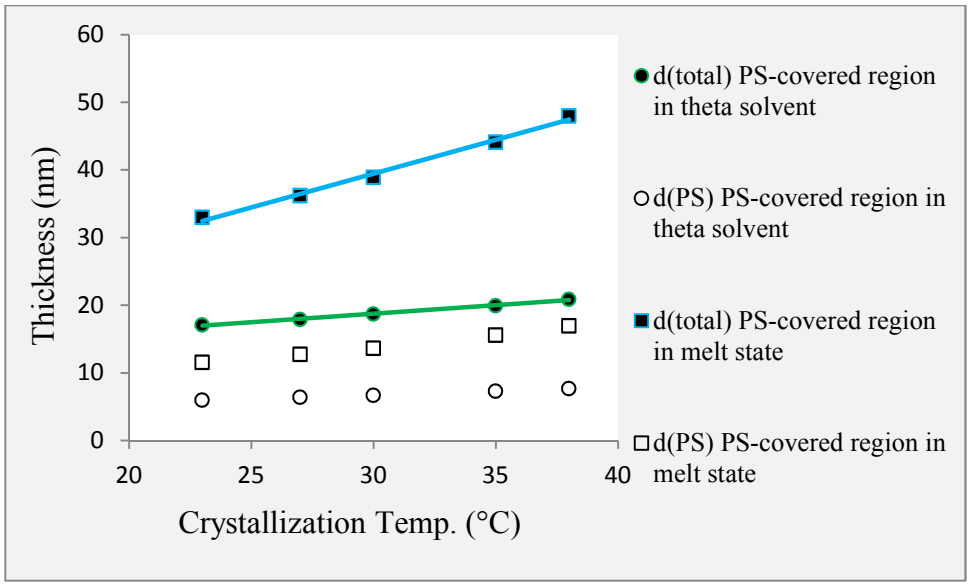

(b)

Fig. 7. Comparison between thicknesses of single crystals grown from theta solvent and polymer melt state at T_c= 23 ºC vs. M_n^{PS} (a); crystallization temperature (b).

Regarding the lateral sizes of the melt- and solution-grown mixed-brush single crystals, the melt grown single crystals were 4 times larger than solution ones (24.04 vs. 6.03 μm). In melt system, due to higher concentration of crystallizable chains, for the same growth time a bigger number of chains can attach to growing seeds, and this leads to greater lateral size.

Conclusions

On the contrary of previous solution-grown mixed-brush single crystals having patterned leopard-skin like surface morphology, the melt-grown ones had co-continuous morphology. The portion of PMMA/PS brushes in solution-grown mixed-brush single crystals (= 20/80) reached to 50/50 in polymer melt-grown corresponding mixed-brush single crystals. In theta condition of melt state the conformations of PS and PMMA chains approach to each other and, consequently,

the system's tendency to attract the chains of opposite type increases. This could result in co-continuous surface morphologies with higher ratio of PMMA brushes. Although for higher concentration and, consequently, higher growth rate, the thicknesses were considerably higher than corresponding thicknesses in dilute solution, the trends of thickness change with molecular weight and crystallization temperature were the same. The steeper slopes proved the accelerated kinetic in melt-grown single crystals. In brief, the co-continuous morphologies of mixed-brush single crystals and conspicuous larger thicknesses in the melt state were ascribed to the dominant kinetic effect instead of the thermodynamic effect in dilute solution growth systems.

Notes and references

1. Lahann, J.; Mitragotri, S.; Tran, T. -N.; Kaido, H.; Sundaram, J.; Choi, I. S.; Hoffer, S.; Somorjal, G. A.; Langer, R. *Science*, 2003, *299*, 371.

2. Manos, D.; Flamm, D. Plasma Etching, and Introduction, Academic Press, Inc., New York, 1989.

3. Russel, T. P. *Science*, 2002, *297*, 964.

4. Pan, V.; Wesley, R.; Lvginbuhl, R.; Denton, D.; Ratner, B. *Biomacromolecules*, 2001, *2*, 32.

5. Nagasaki, Y.; Kataoka, K. *Trends Polym. Sci.*, 1996, *4*, 59.

6. Milner, S. T. *Science* 1991, *251*, 905.

7. Motornov, M; Minko, S; Nitschke, M ; Grundke, K; Stamm, M. *Polymeric Materials: Science and Engineering* 2003*, 88,* 264.

8. Zhao, B.; Brittain, W. J. *Progress in Polymer Science* 2000*, 25*, 677.

9. Gong, P.; Wu, T.; Genzer, J.; Szleifer, I. *Macromolecules* 2007*, 40*, 8765.

10. Koutsos, V.; van der Vegte, E. M.; Hadziioannou, G. *Macromolecules* 1999, *32*,1233.

11. Ionov, L.; Zdyrko, B.; Sidorenko, A.; Minko, S.; Klep, V.; Luzinov, I.; Stamm, M. *Macromol. Rapid Commun.*2004, *25*, 260.

12. Johnson, P. A.; Gaspar, M. A.; Levicky, R. *J. Am. Chem. Soc.* 2004, *126*, 9910.

13. Nakashima, H.; Furukawa, K.; Ajito, K.; Kashimura, Y.; Torimitsu, K. *Langmuir* 2005, *21*, 511.

14. Penn, L. S.; Huang, H.; Sindkhedkar, M. D.; Rankin, S. E.; Chittenden, K.; Quirk, R. P.; Mathers, R. T.; Lee, Y. *Macromolecules* 2002, *35*, 7054.

15. Prucker, O.; Rühe, J. *Macromolecules* 1998, *31*, 592.

16. Jordan, R.; Ulman, A.; Kang, J. F.; Rafailovich, M. H.; Sokolov, J. *J. Am. Chem.Soc.* 1999, *121*, 1016.

17. Vidal, A.; Guyot, A.; Kennedy, J. P. *Polym. Bull.* 1980, *2*, 315.

18. de Bore, B.; Simon, H. K.; Werts, M. P. L.; van der Vegte, E. W.; Hadziioannou,G. *Macromolecules* 2000, *33*, 49.

19. Weimer, M. W.; Chen, H.; Giannelis, E. P.; Sogah, D. Y. *J. Am. Chem. Soc.* 1999, *121*, 1615.

20. Ejaz, M.; Yamamoto, S.; Ohno, K.; Tsujii, Y.; Fukuda, T. *Macromolecules* 1998, *31*, 5934.

21. Matyjaszewski, K.; Miller, P. J.; Shukla, N.; Immaraporn, B.; Gelman, A.;Luokala, B. B.; Siclovan, T. M.; Lickelbick, G.; Vallant, T.; Hoffmann, H.; Pakula,T. *Macromolecules* 1999, *32*, 8716.

22. Weck, M.; Jackiw, J. J.; Rossi, R. R.; Weiss, P. S.; Grubbs, R. H. *J. Am. Chem.Soc.* 1999, *121*, 4088.

23. Hertler, W. R.; Sogah, D. Y.; Boettcher, F. P. *Macromolecules* 1990, *23*, 1264.

24. Zhao, B. *Polymer* 2003*, 44*, 4079.

25. Minko, S.; Patil, S.; Datsyuk, V.; Simon, F.; Eichhorn, K.-J.; Motornov, M.; Usov, D.; Tokarev, I.; Stamm, M. *Langmuir* 2002, *18*, 289.

26. Minko, S.; Usov, D.; Goreshnik, E.; Stamm, M. *Macromol. Rapid Commun.* 2001, *22*, 206.

27. Minko, S.; Müller, M.; Usov, D.; Scholl, A.; Froeck, C.; Stamm, M. *Phys. Rev. Lett.* 2002, *88*, 035502.

28. Zhao, B.; Brittain, W. J. *Macromolecules* 2000, *33*, 8813.

29. Minko, S.; Müller, M.; Motornov, M.; Nitschke, M.; Grundke, K.; Stamm, M. *J. Am. Chem. Soc.* 2003, *125*, 3896.

30. Lemieux, M.; Minko, S.; Usov, D.; Stamm, M.; Tsukruk, V. V. *Langmuir* 2003, *19*, 6126.

31. Wang, J.; Kara, S.; Long, T. E.; Ward, T. C. *J. Polym.Sci., Part A: Polym. Chem.* 2000, *38*, 3742.

32. Zhang, J.; Yang, Y.; Zhao, C.; Zhao, H. *Journal of Polymer Science Part A: Polymer Chemistry* 2007*, 45*, 5329.

33. Abbaspoor, S.; Abbasi, F.; Agbolaghi, S. RSC Advances 2014, *4*, 17071.

34. Minemawari, H.; Yamada, T.; Matsui, H.; Tsutsumi, J.; Haas, S.; Chiba, R.; Kumai, R.; Hasegawa, T. *Nature Letter* 2011, *475*, 364.

35. Jiang, X.; Liu, X.; Liao, Q.; Wang, X.; Yan, D.D.; Huo, H.; Li, L.; Zhou, J.J. *Soft Matter*, 2014, *10*, 3238.

36. Agbolaghi, S.; Abbasi, F.; Abbaspoor, S. *Colloid and Polymer Science* 2014, 292, 1375.

37. Abbaspoor, S.; Abbasi, F.; Agbolaghi, S. *J Polym. Res.* 2014, 21:493, 1.

38. Lotz, B.; Kovacs, A. J. *Colloid Polym. Sci.* 1966, *209(2)*, 97.

39. Lotz, B.; Kovacs, A. J.; Bassett, G. A.; Keller, A. *Colloid Polym. Sci.* 1966, *209*, 115.

40. Vidotto, G.; Lévy, D.; Kovaes, A. J. *Colloid Polym. Sci.* 1969, 230, 1.

41. Blundell, D. J., A. Keller, and A. J. Kovaes, *J. Polymer Sci. B* 1966, *4*, 481.

42. Stephen Z. D. Cheng, H. S. But and Bernhard Wunderlich. *Polymer* 1988, *29*, 579.

43. Cheng, S. Z. D.; Chen, J; Janimak, J. J. Polymer 1990, *31*, 1018.

44. G. Vidotto, D. Lévy; Kovacs A. J. *Kolloid-Zeitschrifl und Zeitschrift für Polymer* 1969, *230*, 289.

45. Geil, P. H. (1963*)* Polymer Single Crystals, Interscience, New York/London.

46. Agbolaghi, S; Abbasi, F; Abbaspoor, S. *Polym. Bull.* 2014 (submitted).

47. Agbolaghi, S; Abbasi, F; Jalili, K. *J Polym. Res.* 2014, *21:380*, 1.

48. Chen, Y. Dissertation, University of Akron, 2005.

49. Van Horn, R. M. Ph.D. Dissertation, University of Akron, 2009.

50. Cauda, V.; Argyo, C. H.; Bein, T. H. *J. Mater. Chem.* 2010, *20*, 8693.

51. Zheng, J. X.; Xiong, H.; Chen, W.Y.; Lee K.; Van Horn, R. M.; Quirk, R. P.; Lotz, B.; Thomas, E. L.; Shi, A. -C.; Cheng, S. Z. D. *Macromolecules* 2006, *39*, 641.

52. Brandup, J.; Immergut, E. H. Polymer Handbook; Wiley: New York, 1975.

53. Rubinstein, M.; Polymer physics; Oxford university press, 2003.

54. Sperling, L. H.; Introduction to physical polymer science, John Wiley, 2006.

55. Hoffman, J. D.; Lauritzen, J. I. *J. Res. Natl. Bur. Stand.* 1961, *65A*, 297.

56. Wunderlich, B. *Macromolecular Physics*; Academic Press: New York, 1980.

57. Lauritzen, J. I.; Hoffman, J. D. *J. Res. Nat. Bur. Std*. 1960, *64A*, 73.

58. Fetters, L. J.; Hadjichristidis, N.; Lindner, J. S.; Mays, J. W. *J. Phys. Chem.* 1994, 23, 619.

59. Kent, M. S. *Macromol. Rapid Commun.* 2000, 21, 243.

60. DiMarzio, E. A.; Guttman, C. M.; Hoffman, J. D. *Macromolecules* 1980, *13*, 1194.

61. W. Y. Chen, J. X. Zheng, S. Z. D. Cheng, C. Y. Li, P. Huang, L. Zhu, H. Xiong, Q. Ge, Y. Guo, R. P. Quirk, B. Lotz, L. Deng, C. Wu and E. L. Thomas, Phys. Rev. Lett., 2004, *93*, 028301.

62. Keller, A.; O'Connor, A. *Disc. Faraday Soc.* 1958, *25*, 114.

63. Wunderlich, B. *Macromolecular Physics* Vol. 1: Crystal Structure, Morphology, defects, Academic, New York, 1973.

64. Kovacs, A. J.; Gonthier, A. Colloid Polym. Sci. 1972, *250*, 530.

65. Ruland, W. *Colloid Polym Sci* 1977, *255*, 417.

66. Stribeck, N.; Ruland, W. *J. Appl. Crystallogr.* 1978, *11*, *535.*

67. Hamie, H. PhD Dissertation, University of Haute Alsace 2010.